An integrated approach combining soil profile, records and tree ring analysis to identify the origin of environmental contamination in a former uranium mine (Rophin, France)

A. Martin, Y. Hassan-Loni, A. Fichtner, O. Péron, Karine David, P. Chardon, S. Larrue, A. Gourgiotis, S. Sachs, T. Arnold, et al.

An integrated approach combining soil profile, records and tree ring analysis to identify the origin of environmental contamination in a former uranium mine (Rophin, France)

A. Martin[a], Y. Hassan-Loni[a], A. Fichtner[a,b], O. Péron[a,*], K. David[a], P. Chardon[c], S. Larrue[d], A. Gourgiotis[e], S. Sachs[b], T. Arnold[b], B. Grambow[a], T. Stumpf[b], G. Montavon[a]

*Corresponding author: olivier.peron@subatech.in2p3.fr

Phone: +33 2 51 85 86 26

[a] Laboratoire SUBATECH, UMR 6457, IMT Atlantique/Université de Nantes/CNRS/IN2P3
4 Rue Alfred Kastler, 44307 Nantes, France

[b] Helmholtz-Zentrum Dresden - Rossendorf, Institute of Resource Ecology,
Bautzner Landstraße 400, 01328 Dresden, Germany

[c] LPC, UMR 6533, CNRS/Université Clermont Auvergne, 4, rue Ledru,
63057 Clermont-Ferrand cedex, France

[d] GEOLAB, UMR 6042, CNRS/Université Clermont Auvergne, 4, rue Ledru,
63057 Clermont-Ferrand cedex, France

[e] Institut de Radioprotection et de Sûreté Nucléaire - PSE/ENV - SEDRE/LELI,
Fontenay-aux-Roses, 92262 France

Highlights

- Origin of contamination near Rophin tailings storage site: natural vs. anthropogenic
- A whitish silt loam soil layer in a wetland was associated with a high U content.
- Dating and records indicate that U was deposited during previous mining activities.
- U mineral particles transported by turbid waters were deposited in a wetland.
- Dendroanalysis shows an uptake of ^{238}U linked to the mining activity period.

Abstract

Uranium mining and milling activities raise environmental concerns due to the release of radioactive and other toxic elements. Their long-term management thus requires a knowledge of past events coupled with a good understanding of the geochemical mechanisms regulating the mobility of residual radionuclides. This article presents the results on the traces of anthropic activity linked to previous uranium (U) mining activities in the vicinity of the Rophin tailings storage site (Puy de Dôme, France). Several complementary approaches were developed based on a study of the site's history and records, as well as on a radiological and chemical characterization of soil cores and a dendrochronology. Gamma survey measurements of the wetland downstream of the Rophin site revealed a level of 1,050 $nSv.h^{-1}$. Soil cores extracted in the wetland showed U concentrations of up to 1,855 $mg.kg^{-1}$, which appears to be associated with the presence of a whitish silt loam (WSL) soil layer located below an organic topsoil layer. Records, corroborated by prior aerial photographs and analyses of ^{137}Cs and ^{14}C activities, suggest the discharge of U mineral particles while the site was being operated. Moreover, lead isotope ratios indicate that contamination in the WSL layer can be discriminated by a larger contribution of radiogenic lead to total lead. The dendroanalysis correlate U emissions from

Rophin with the site's history. Oak tree rings located downstream of the site contain uranium concentrations ten times higher than values measured on unaffected trees. Moreover, the highest U concentrations were recorded not only for the operating period, but more surprisingly for the recent site renovations as well. This integrated approach corroborates that U mineral particles were initially transported as mineral particles in Rophin's watershed and that a majority of the deposited uranium appears to have been trapped in the topsoil layer, with high organic matter content.

Graphical abstract

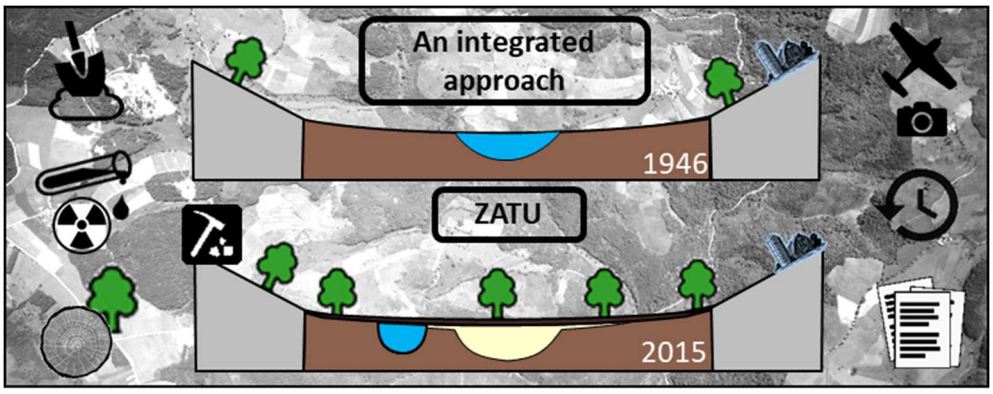

Keywords

Uranium mining, wetland, records, dendroanalysis, radiochronology, U decay chain.

1. Introduction

Uranium (U) is a key resource that has been mined in France for use in the nuclear energy industry from 1948 to 2001. Uranium mining and milling activities, as well as mineral processing plants, raise environmental concerns due to the possible release of radioactive and other potentially toxic elements (Ljungberg and Öhlander, 2001; Lottermoser and

60 Ashley, 2005). The impact of U release into the environment is governed by the U speciation,
61 which influences its solubility, mobility and bioavailability (Abdelouas, 2006). In areas
62 unaffected by human activity, the inflow of U is considered to be primarily related to its
63 dissolved or colloidal species; in the vicinity of mines on the other hand, its transport can
64 also occur in the form of U mineral particles. Even though in Western Europe most U mines
65 were shut down over the course of the past few decades, these former mines and especially
66 their associated tailings storage sites are subject to continuous environmental monitoring
67 (Ballini et al., 2020). In addition to the environmental monitoring of storage sites, it is also
68 critical to consider the environment potentially contaminated near the mines. This
69 consideration becomes even more important since the land may now be privately owned
70 (Mangeret *et al.*, 2018).

71 In the vicinity of U mines, wetlands prove to be particular natural zones since they act as
72 physical particle and metal traps. Numerous studies have indeed found highly increased U
73 concentrations in wetlands, extending into the several thousand $mg.kg^{-1}$; this observation
74 has been recorded in areas affected by mining activities (Li et al., 2014; Mangeret et al.,
75 2018; Schöner et al., 2009; Wang et al., 2014) as well as areas with granitic bedrock
76 subjected to naturally elevated U concentrations in groundwater (Mikutta et al., 2016; Owen
77 and Otton, 1995; Regenspurg et al., 2010; Zielinski et al., 1986). The accumulation of U is
78 explained by complexation with organic matter (OM) present at high concentrations in
79 wetlands (Bordelet et al., 2018) and/or by reduction of U(VI) to scarcely soluble U(IV) due to
80 strongly reducing conditions related to the bacterial degradation of plant material (Alessi et
81 al., 2012; Cumberland et al., 2016; Lovley et al., 1991; Nakashima et al., 1984; Newsome et
82 al., 2015). However, it must be noted that the observed contaminations may be of natural

83 origin, without the involvement of any human action. Weathering and erosion of the local
84 bedrock, which is often granitic in the case of French U mines, can also play a major role in
85 increasing these concentration levels. High U contents have in fact already been
86 documented at sites not heavily impacted by mining activities, such as Alpine soils (up to
87 4,000 $mg.kg^{-1}$), or by ground and surface waters, where the surrounding bedrock mainly
88 consists of crystalline rocks that commonly contain trace amounts of U (Gourgiotis *et al.*,
89 2020).

90 It is essential to not only report any past contamination linked to uranium mining, but also
91 trace the origin of such contamination over these sites, i.e. natural vs. anthropogenic. This
92 question corresponds to the focus of this article combining different approaches, featuring
93 both direct knowledge of past events and an analysis of the records or characterization of
94 environmental indicators like soil and vegetation.

95 In the absence of first-hand recollections of details surrounding the period of operations (Le
96 Berre and Bretesché, 2019), the knowledge of past contaminations requires a rigorous study
97 of historical evidence, mostly documents (regulatory and technical reports) and, ideally, a
98 direct consultation of various records like raw data without operator interpretation. For
99 example, a study of site history combined with satellite images or previous aerial
100 photographs has been used to determine how tailings were deposited in ponds, e.g. disposal
101 of tailings at the Cominak mine in Niger (Déjeant et al., 2016) or at the Bois Noirs mine in
102 France (Chautard et al., 2020).

103 Concerning the soil analysis, an initial possibility consists of correlating the observed
104 contaminations with dating approaches, i.e. ^{137}Cs and/or ^{14}C (Cuvier *et al.*, 2016). It should
105 be noted that excessive use of ^{210}Pb is unfortunately impossible in a U mining context (Reyss

106 *et al.*, 2016). The origin of these U markings, whether natural or anthropogenic, can then
107 also be traced by means of lead isotopy (Bollhöfer, 2012; Bollhöfer *et al.*, 2006; Cuvier *et al.*,
108 2016; Gourgiotis *et al.*, 2020).

109 Concerning vegetation, past contaminations can be retrieved through dendroanalysis. This
110 step consists of measuring the distribution of trace elements in the annual growth rings of
111 trees; it is based on the assumption that trace elements remain immobile once deposited in
112 the stem. Such a premise has raised controversy in the literature (Hagemeyer, 2000; Nabaisa
113 et al., 1999). The method has been implemented on a variety of tree species in order to
114 correlate trace metal concentrations with the pollution history at various locations
115 (Beramendi-Orosco et al., 2013; Pearson et al., 2005; Watmough and Hutchinson, 1996). The
116 Cornish oak, *Quercus petraea*, has been repeatedly reported as a suitable indicator of
117 changes in bioavailable trace metal concentrations in an environment with trees over time
118 (Cutter and Guyette, 1993; Jonsson et al., 1997; Perone et al., 2018). Furthermore, oak tree
119 rings have been tested for use in biomonitoring uranium (Edmands et al., 2001), specifically
120 in the vicinity of former mining activities (Märten et al., 2015; Monticelli et al., 2009). This
121 approach however accounts for contamination by soluble, hence bioavailable, metals with
122 root capture generally being predominant (Lepp, 1975).

123 In summary, several complementary approaches are possible, each providing information, to
124 characterize the origin of past contaminations. The ambition of this work is therefore to
125 combine all these approaches to assess the origin of a contaminated wetland around the
126 Rophin site (Puy-de-Dôme, France). Among the 16 sites chosen to store U waste in France
127 (IRSN, 2018) and, as such, classified as an ICPE installation necessitating environmental
128 protections, it was recently integrated into France's network of pilot study zones, under the

ZATU (*Zone Atelier Territoires Uranifères*) created in 2015. This network is part of the Long-Term Ecosystem Research ongoing in Europe (Bretagnolle et al., 2019). In this work, the results obtained from surface gamma surveys are compared with soil core analyses (lead isotopy, dating approaches, uranium and decay products) and dendrochronology, as well with information obtained from mine operating history through reliance on different sources in order to reconstitute the events leading to the current state of the Rophin site and its immediate environs.

2. Study site

The Rophin site lies within the Forez range east of the Limagne Graben, in the northeastern part of the Puy de Dôme department, close to the city of Lachaux (Fig. S1) and was among several mines referenced as Western Lachaux ore bodies (Fig. S2). In this area, the mean annual, temperature is 10.1°C with mean annual precipitations of 800 mm y^{-1} (Météo-France, www.meteofrance.com). In the global context, Western Lachaux ore bodies appear as exceptional due to the predominance of parsonsite ($Pb_2(UO_2)(PO_4)_2$, 2H2O) under a workable deposit rather than an alteration product of pitchblende. The ore bodies are hosted by coarse-grained peraluminous granite of the alkaline type, like “Bois Noirs” granite, situated at the end of Variscan orogeny (Fig. S1). These bodies consist of low-temperature silica/quartz containing uranyl phosphate minerals, mainly parsonsite and, at the oxidized ore surface, both autunite ($Ca(UO_2)_2(PO4)_2$, 8-12 H_2O) and tobernite ($Cu(UO_2)_2(PO_4)_2$, $12H_2O$) (Greffoy and Sarcia, 1955; Himeur and Andres, 2012). The principal events in the history of the Rophin mine have been summarized in a timeline (Fig. 1) with further details in Fig. S3.

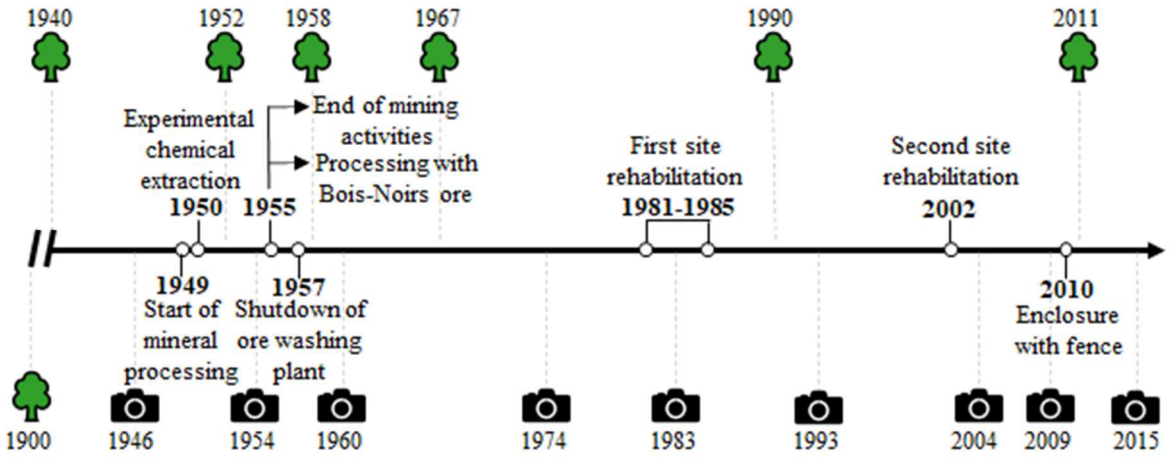

Fig. 1: Timeline of Rophin mine operations with time-stamped aerial photographs (Fig. S6) and the sampling strategy for tree ring analysis

To treat the materials extracted in the Western Lachaux sector, a mechanical ore washing plant was built in 1948 next to the Rophin mine (Fig. S4 and Fig. S5). At first, ore treatment was gravimetric with a vibrating table, crushing machines and a flotation circuit that included 3 settling ponds to retain U particles (Himeur and Andres, 2012). In all, fewer than 30 tons of U were extracted from mine tailings, at a mean concentration rate of 0.7‰, and then exported as 4.4% concentrates. Over 30,000 tons of mine and mill tailing waste were stored on the site of the former processing plant (ICPE, see hachured area in Fig. 2).

Nowadays, the storage site is covered by vegetated soil, and forest vegetation is growing at the top of the mine waste storage heap. Periodic water effluents from the underground galleries are collected in a trench located in the western part of the Rophin ICPE. These effluents join the “Le Gourgeat” stream heading in a NW-S direction; the stream is connected to the five local ore bodies in the same watershed and moreover contributes to the formation of a local wetland 200 m downstream of the Rophin site (Fig. S4). During the period of mining operations, the Gourgeat watershed was closed 2 km downstream of the Rophin site by a dam used as a water storage reservoir for water supply of the upper ore

washing plant before its ultimate connection with the Terrasson stream. A general map of the Gourgeat watershed, with other former U mines, is presented in Fig. S2. A biannual control of the uranium and radium concentrations in the effluent waters was set up as part of the ICPE site supervision program. Moderately high aqueous U concentrations have been detected in the trench collecting effluent waters running inside the ICPE, with values at times reaching 200 $\mu g.L^{-1}$ (Himeur and Andres, 2012).

The former Rophin mine has been chosen as study site for a variety of reasons. It is now uninhabited where vegetation grows on mine tailings, stored *in situ*, coupled with the presence of a creek (Gourgeat) running in the watershed and a wetland downstream of the storage area. The site offers a framework for conducting multidisciplinary scientific investigations on life under natural radioactivity in ZATU context.

3. Materials and Methods

3.1. Methodology for studying the history of mining operations

Generally speaking, French U mine operations have often been overlooked by residents (Le Berre and Bretesché, 2019), and former operators (CEA, COGEMA, AREVA and now ORANO) owned most of the records. In an effort to retrace the history of site operations as accurately as possible, several data sources were consulted:

(i) A compilation of data retracing the site history through: the operator's archivist and mine specialists (Guiollard, 2002), regulatory reports on environmental monitoring (Himeur, 2010; Himeur and Andres, 2012), technical reports on mine operations (Greffoy and Sarcia, 1955), and other independent environmental associations (Commission for Independent Research and Information on RADiation and the Puy de Dôme environment association).

(ii) A direct consultation of the records held by the Auvergne-Rhône-Alpes DREAL (Regional Directorate for the Environment, Land Planning and Housing) made available for onsite consultation in February and March 2017. These documents contain raw uninterpreted data from operators, including administrative and regulatory documents, inspection reports, correspondence between operators and oversight agencies, press articles and documents relative to mine operations (map, fees, etc.). A summary of the documents consulted, arranged in chronological order, is available in Fig. S3, Fig. S5 and Table S14.

(iii) A collection of aerial photographs available from the "Geoportail" database (National Geographic Institute (IGN)), allowing for observations of the site before, during and after mining operations (Fig. S6). Nine archived aerial photographs, with a spatial resolution of 50 $cm.pixel^{-1}$ and a planimetric accuracy of less than 2 m, were projected into a WGS84 (World Geodetic System 1984) using QGIS (Quantum Geographic Information System).

The results from the analysis of these selected documents, that enable tracing the history of site operations, will be summarized in the following section (3.1). These data will then be discussed in light of field measurement results obtained from our two centers of interest, i.e. wetland soils and tree rings.

3.2. Sampling strategy

An environmental monitoring and sampling campaigns were carried out between 2014 and 2018 (Fig. 2).

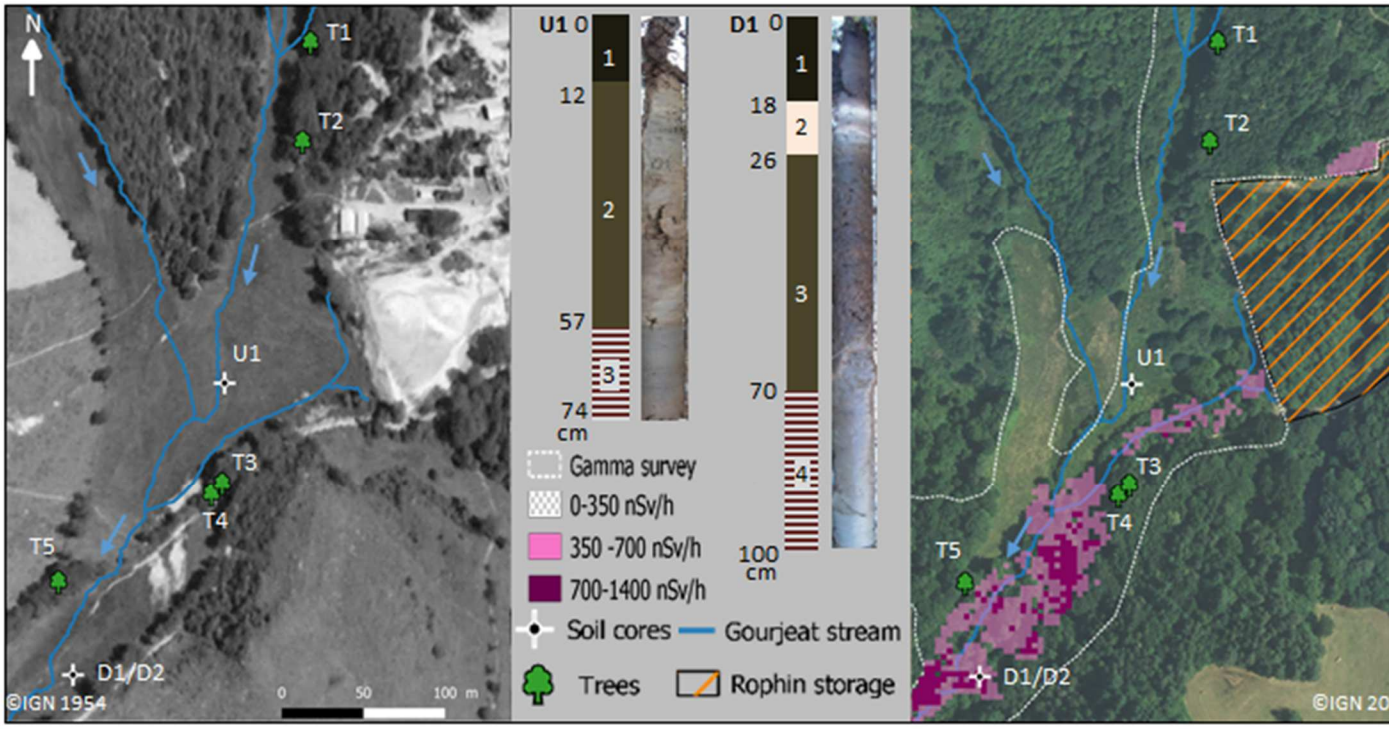

Fig. 2: Overview of the Gourgeat watershed with sampling locations. Left: Aerial photograph (1954) with the Rophin mine processing plant. Right: Aerial photograph (2015) of the ICPE site with interpolated gamma dose rates. Center: Photographs and soil profile descriptions of cores U1 and D1 over 74 and 100 cm. A second core (D2) with a higher vertical resolution was collected in April 2018.

3.2.1. Gamma survey

A radiological survey of the Gourgeat watershed was performed to provide an overview of the dose rate distribution at the periphery of the ICPE site open to the public. Dose-rate mapping (Fig. 2 and Fig. S4) was obtained with SG-2R gamma-ray sensors (Canberra, Inc.). The device used coupled the gamma-ray sensor (energy range: 59 keV to 1.5 MeV, and measurement range: 10 $nSv.h^{-1}$ to 1 $mSv.h^{-1}$) with a Colibri® device (Canberra, Inc.) featuring an integrated GPS. Data were acquired automatically every 5 s or 30 s directly in dose rate, and the sensors were placed approx. 1 m above ground. The measurements were conducted during 5 field campaigns, from December 2014 to June 2018, across different areas. The measured data points, reported in $nSv.h^{-1}$ (80 - 1,050 $nSv.h^{-1}$), were interpolated with the

225 inverse distance weighting method (distance coefficient = 5) using the QGIS software
226 interpolation tool.

227 ***3.2.2. Soil sampling***

228 Two soil cores were collected in January 2016 at locations upstream (Core U1) and
229 downstream (Core D1) of the hydraulic system (Fig. 2) in place to assess the environmental
230 footprint of the Rophin site with a Russian corer 100 cm long and 5 cm in diameter
231 (Eijkelkamp). Cores U1 and D1 were brought back to the laboratory, subsampled with a
232 cleaned ceramic blade the next day into 2-cm sections under laboratory atmosphere and
233 lyophilized for gamma spectrometry analysis, ^{14}C dating and lead isotopy. A second
234 downstream core (D2) with a greater vertical resolution (Fig. 2) was collected in April 2018
235 close to the D1 location (Fig. S5c) with an in-house corer developed to protect the sample in
236 a plastic tube (8.5-cm inner diameter, Fig. S7). After extraction, the core was stored at -20°C
237 in a mobile freezer. Once back in the laboratory, the frozen core was cut into 1-cm slices by
238 means of a bandsaw. Two subsamples from core D2 were analyzed by Scanning Electron
239 Microscopy (SEM) and Energy Dispersive X-Ray Spectroscopy (EDS) according to the
240 methodology explained in Fig. S8 to determine location of U within minerals.

241 In addition, a total of 17 cores, called the M-series, were extracted in April 2018 (Russian
242 corer, 50 cm, Eijkelkamp) over a distance of about 300 m alongside the main creek running
243 from the storage site in order to provide an overview of the soil profile in the wetland (Fig.
244 S9). Following core extraction, 2 to 4 sections of approx. 5 cm were selected depending on
245 the soil profile, subsampled with the same protocol than for D1 core, and then stored in 250-
246 mL plastic jars for gamma spectrometry analysis.

3.2.3. Tree sampling

Tree ring samples were collected from five oak trees (*Quercus petraea*), chosen for their age estimated at more than 100 years (T1 to T5) and located between 50 and 200 m from the former uranium mining and storage residue (Fig. 2). Trees T1 and T2, located upstream in the vicinity of the storage residue, are not influenced by the Gourgeat watershed due to an elevation difference exceeding 10 m. Trees T3 and T4, growing downstream of the storage residue, are located in the watershed very close to the site of water runoff from the storage residue. The last tree sampled, T5, is located further away, 200 m downstream of the storage residue, and has no apparent connection with the watershed due to elevation difference (Fig. 2, Fig. 6 and Table S10).

Tree rings were collected on each tree using an increment borer (Pressler; inner diameter 5 mm). The selected trees were healthy, grew under similar surrounding natural conditions and belonged to the same cohort. The samples were extracted from the trunk at roughly 1.5 m above ground in July 2015. Sampling was performed with great care so as to avoid any cross-contamination, i.e. the borer was washed with ethanol and Milli-Q water between each extraction. After sampling, all cores were immediately sealed in plastic tubes and transported to the laboratory for dendroanalysis. The samples were dried at room temperature and polished with sandpaper to improve visibility of the growth rings. To avoid any cross-ring contamination, the samples were cleaned by removing any dust with compressed air. Tree ring samples were then scanned (1,600 dpi), and the CooRecorder software (Larsson, 2016) was run for age determination with a final uncertainty of ±1 year. The period covered by the tree rings ranged between 118 and 176 years (Table S10). Seven different years were selected for U analysis (Fig. 1): years 1900 and 1940 were chosen to

represent the period before mining activity; 1952 for the period of operations; 1958 for the mine's closure; and 1967, 1990 and 2011 for the period subsequent to specific site rehabilitation works.

3.3. Analysis

3.3.1. Gamma spectrometry

Soil radionuclide contents from the ^{238}U decay chain (^{234}Th, ^{226}Ra, ^{210}Pb) were analyzed by means of gamma spectrometry. These analyses were carried out in filled petri dishes (5 cm diameter, 1.5 cm thick) sealed in a radon protection membrane (Petri-Seal$^{(TM)}$). The samples were first analyzed for 3 hours and then 10 hours for those with low activity. The gamma spectrometry was performed using HPGe-detectors (Canberra, BE4823/S) with a high purity germanium detector (Ge-crystal, 7500SL cryostat, 2002CPSL pre-amplifier) and a multi-channel analyzer (MCA). Energy calibration by a ^{152}Eu certified source (peak energy range: 122 to 1408 keV) has been coupled to a certified multigamma mixture for efficiency (peak energy range: 60 to 1,836 keV). A multigamma mixture (^{241}Am,^{109}Cd ^{57}Co, ^{139}Ce, ^{51}Cr, ^{113}Sn, ^{85}Sr, ^{137}Cs, ^{60}Co, ^{88}Y) has been proportionally introduced so that the counts for each of the energies are equivalent. The self-absorption of gamma lines in materials was taken into account in the Labsocs software using the composition and density of a typical soil sample. All radionuclide concentrations are expressed with uncertainties at 2σ. These concentrations (^{234}Th, ^{226}Ra, ^{210}Pb) with LD (^{210}Pb) = 35.2 Bq.kg^{-1}; LD (^{226}Ra) = 52.0 Bq.kg^{-1}; LD (^{234}Th) = 34.6 Bq.kg^{-1}) were respectively determined with the following energy signals: 63.3 keV, 186.1 keV, and 46.5 keV. The ^{238}U sample concentrations were determined by assuming a secular equilibrium in the head of the decay chain between ^{234}Th and ^{238}U. The resulting ^{238}U concentrations were calculated with a specific activity of 12,350 Bq.g^{-1}.

The 186.1 keV energy signal of ^{226}Ra interferes with the 185.7 keV energy signal of ^{235}U; this effect is corrected by introducing the ^{235}U concentration predicted by the natural isotopic ratio from ^{238}U concentrations. The ^{226}Ra values were verified for a few samples by measuring radiochemical equilibrium with its daughter nuclide ^{214}Pb (295.2 keV, 351.9 keV; $LD = 13.2\ Bq.kg^{-1}$) and ^{214}Bi (609.3 keV, 1120.3 keV, 1764.5 keV; $LD = 81.4\ Bq.kg^{-1}$) by using sealed samples (to prevent radon from escaping) stored for at least 3 weeks. Equilibrated samples were used for the ^{210}Pb activity determination. In addition to analyzing the ^{238}U decay chain, the ^{137}Cs (661.7 keV) was measured for 24 h in a low-background environment, according to the protocol developed by Tedjani et al., (2016) in order to both achieve a lower limit of detection (2 $Bq.kg^{-1}$) and perform soil dating over the depth.

3.3.2. Water and soil organic matter content

Water and soil organic matter (SOM) contents of soil samples were simply determined by loss on ignition; this procedure relied on the protocol found in Heiri et al., (2001). Between 5 and 10 g of homogenized wet samples were introduced into porcelain crucibles and first dried at 105°C overnight in a furnace (Nabertherm, Inc.), then heated at 550°C for 4 h to burn the organic matter. After each heating step, the crucibles were cooled to room temperature in a desiccator and weighed. SOM content was expressed relative to dry soil content, in contrast with water content, that account for the entire sample mass. The uncertainty for both measurements, expressed as a confidence interval (2σ), was calculated at less than 10%.

3.3.3. ^{14}C dating

Several samples from core D1 were analyzed by applying the Accelerator Mass Spectrometry (AMS) radiocarbon dating technique after graphitization. Results (in age calBP) were

316 obtained by running the software OxCal V4.3.2 (Ramsey, 2017) using the IntCal13
317 atmospheric curve (Reimer et al., 2013). More detailed information is available in Table S11.

318 ***3.3.4. Soil sample preparation and Pb HR-ICP-MS analysis***

319 Lead isotope ratios were analyzed on a single-collector high-resolution ICP-MS instrument
320 (ELEMENT XR, Thermo Scientific, Bremen, Germany) after chemical purification of the lead in
321 soil samples using a Dowex 1x8 (100-200 mesh) anion exchange resin in bromide form.
322 Prior to analysis, 100 mg of soil sample were acid digested using a microwave oven (ETHOS
323 Easy, Milestone) in accordance with the EPA 3051A method drawn from the Milestone
324 application book. Concentrated nitric acid (70% HNO_3, Fisher Scientific) and hydrochloric
325 acid (37% HCl, Fisher Scientific) were purified with the Savillex DST-1000 sub-boiling
326 distillation system. The insoluble residue obtained after sample mineralization (leaching and
327 incomplete digestion) was discarded by centrifugation while the supernatant was
328 evaporated to dryness in a clean environment using the EvapoClean® device (Analab®). The
329 sample was dissolved with 2 mL of 0.5 M HBr prepared from a high purity, concentrated HBr
330 acid (Optima grade, Fisher Scientific), centrifuged and loaded onto the 1.2-mL ion exchange
331 column to separate major cations with additional HBr and 0.5 M HCl, plus the elution of lead
332 with 2 mL of 6 N HCl into a 5-mL Savillex vial. The average procedural Pb blank of 1.0 ± 1.6 ng
333 (2σ, n=12) is lower by a factor ranging from 1,500 to 75,000 relative to the amount of Pb
334 derived from soil samples. Preliminary quantitative Pb analyses of the collected sample
335 fractions were carried out in order to prepare sample solutions at a Pb concentration of 2 ng
336 mL^{-1} in 2% HNO_3 (v/v) for Pb isotope measurements performed by means of HR-ICP-MS.

337 All stable lead isotopes (^{204}Pb, ^{206}Pb, ^{207}Pb, ^{208}Pb) and mercury isotopes (^{201}Hg, ^{202}Hg) were
338 measured with the operating and data acquisition parameters detailed in Table S12. The

analysis sequence consisted of five replicate analyses of the unknown sample solution bracketed by five replicate analyses of a 2 $\mu g.L^{-1}$ Pb solution of the NIST SRM981 Pb isotope standard with, between them, the 2% HNO_3 (v/v) blank solution analysis. The isobaric interference from ^{204}Hg on ^{204}Pb was corrected using the measured signal intensity of ^{202}Hg, and the abundance ratio $^{202}Hg/^{204}Hg$ equaled 4.35. Special attention was paid by measuring the additional ^{201}Hg, yielding the ratio of signal intensity of both isotopes with respect to the abundance ratio $^{202}Hg/^{201}Hg$ and showing evidence of spectral interference free Hg isotopes. The Pb isotope ratios ($^{204}Pb/^{206}Pb$, $^{207}Pb/^{206}Pb$, $^{208}Pb/^{206}Pb$) were corrected for instrumental mass discrimination using the exponential law (Fig. S13). The mass bias factor applied to the five replicate analyses of an unknown sample is the average of such factors calculated from analyses of the NIST SRM981 Pb both before and after the sample analyses. The errors calculated on Pb isotope ratios in soil samples correspond to two standard deviations from the mean (2σ) based on five replicate analyses of the same sample solution.

3.3.5. Tree sample preparation and U HR-ICP-MS analysis

Individual rings were cut out using a sterilized scalpel that was washed with high purity ethanol and 5% HNO_3 (v/v); this step was followed by a Milli-Q wash in between cuts. The obtained sample weights varied from 10 to 40 mg. The digestion procedure has been described elsewhere (Hassan Loni et al., 2019) and proves to be suitable for low-mass samples. The wood sections were washed in 0.1 M HNO_3 for about an hour and then dried in an oven for 7 h at 70°C (until achieving constant weight). Next, the samples were weighed and deposited in a 5-mL Savillex container, with 1 mL of concentrated HNO_3 being added. The containers were placed in an oven at 80°C for one day; 0.5 mL of ultrapure 30% H_2O_2 were added and the samples placed back in the oven for one more day. The solutions were then cooled and diluted in 2% HNO_3 (v/v) using the ^{205}Tl internal standard working solution

363 prepared at a concentration of 50 ng.L^{-1}. The suitability and accuracy of this method were
364 tested through a digested standard reference material, i.e. SRM NIST 1570a spinach leaves
365 (U content = 0.155 ± 0.023 mg.kg^{-1}) according to the same procedure.

366 The U concentrations in tree ring sample solutions obtained after digestion were measured
367 by means of the HR-ICP-MS. The optimized ICP-MS operating conditions are given in Table
368 S12. The calibrated U standards were prepared from 1,000 mg.L^{-1} uranium ICP standard
369 solution (SCP Science). Typical standard calibration curves could be obtained from
370 measurements of the 2% HNO_3 (v/v) blank solution and U standard solutions of 10, 20, 30
371 and 50 ng.L^{-1}. The correlation coefficient (R^2) values over the study duration were between
372 0.999 and 1.00. ^{205}Tl and ^{238}U were measured at low resolution in E-scan acquisition mode,
373 with the detector in triple mode. The limits of detection ranged from 0.002 to 0.2 ng.kg^{-1},
374 and the relative standard deviation (2σ) was < 15%.

4. Results

4.1. Records and maps

4.1.1. Records

Given this setting where mining operations previously encompassed the entire Gourgeat watershed, further details into what actually happens during mining can be gleaned from a study of several records. From selected correspondence, a description of the extracted minerals and residue could be clarified. Some ore bodies contain kaolinite clays, which were detrimental to the ore washing plant process during the sedimentation step and resulted in a loss of U mineral particles with mine tailings (Table S14, 29/06/1948). The discharge waters into the Gourgeat stream after the settling ponds were turbid due to an excess capacity limitation and inadequate maintenance of the facility (i.e. a mix of mud and sand never emptied) (Table S14, 27/10/1950, 21/04/1952, 20/10/1952, 27/07/1953, 26/06/1954). From these letters (Table S14, 12/01/1951, 27/07/1953 and 26/06/1954), we learned that a white coloration of the Terrasson and Vauziron streams over a distance of several kilometers was reported due to fine particles clogging the filters for the abstraction of drinking water to supply the City of Chateldon.

4.1.2. Maps

A study of the 9 available prior aerial photographs from 1946 to 2015 (Fig. S6) has highlighted the changes induced by mining activities on the watershed as regards the timeline events (Fig. 1). Before the mine was founded in 1946, the head of the watershed was a grassland dedicated to breeding with a small stream running through the center. On the 1954 photograph showing mining operations, the footprint of mine installations with settling ponds is clearly visible. A large white deposit in the watershed some 200 m

downstream of the hydraulic output of the Rophin settling ponds can be noticed. Moreover, the small stream is highlighted by a white color, in comparison with the photographs from 1946. The mine was then abandoned and overrun by vegetation (Fig. S6, 1960 and 1974). The first site rehabilitation is visible on the 1983 picture, with a large forest clearing on the mine for the purpose of dismantling the former installations. This step was repeated (visible in the 2004 photo) for the erection of a fence in 2015 in order to secure the ICPE installation. Since 1960, the vegetation growing in the watershed downstream of the mine has now become forestland.

4.2. Gamma survey results

Results from the gamma survey are reported in Fig. 2 as a gamma cartography with 3 radioactivity levels. The measured gamma dose rates range from 80 to 1,050 $nSv.h^{-1}$ in following a Gaussian distribution pattern for values between 80 and 350 $nSv.h^{-1}$. Regarding the wider area under investigation, this pattern was assumed to be the local geological background (GB) of the Rophin area, with a mean value of 210 $nSv.h^{-1}$, which aligns with a regional background between 201 and 250 $nSv.h^{-1}$ measured by IRSN, (2014). From this initial observation, two additional radioactivity levels were defined as 1-2 times and 2-4 times the geological background (i.e. 350-700 and 700-1,400 $nSv.h^{-1}$) in order to facilitate the reading of interpolated results on the gamma cartography.

The northern part of the ICPE area and the two creeks running from the north, which supply water to the wetland area, show values around the level of the GB. In the eastern part of the map, from the effluent waters discharged by the ICPE, a level of 1-2 GB was measured. The gamma radiation level then increases to 1-4 GB (maximum at 1,050 $nSv.h^{-1}$) in the watershed after the confluence of the Gourgeat creek from the north and ICPE effluent waters (Fig. 2).

This high gamma dose rate level was localized on the valley floor, characteristic of a wetland, along the stream within a wide surrounding area without any clear pattern for maximum values. This gamma survey served as the basis for implementing the soil sampling strategy.

4.3. Soil analysis

4.3.1. Soil properties

The U1 soil core was sampled in the upstream grassland, whereas D1 and D2 were sampled in a wooded wetland fully saturated by water during a high flow period (Fig. 2). Consequently, these soil layers were considered at their maximum water holding capacity.

By observation of the D1 core (Fig. 2 and Fig. 3), 4 layers can be distinguished, based on visual criteria and soil organic matter (SOM) content. The top of the core (D1-1; 0-18 cm) consists of black soil composed of fibrous material and roots with a very high water content (78% of total mass) and SOM (34% of dry mass). At a depth between 18 and 30 cm (D1-2), the soil layer features a whitish color with a silt loam texture, a low organic content (8%) and a water content dropping to minimum value of 26%. The next layer (D1-3; 30-70 cm) is characterized by a brown color and a high organic carbon content (45%), which suggests a more heavily decomposed organic matter than in the D1-1 layer. The last brown-gray soil layer (D1-4; 70-100 cm) comprises a mix of organic and mineral characteristics, with a low level of SOM (7%), an apparent silt loam texture and a decreasing water content with depth (from 83% to 18%). The water and SOM contents of core D2 at the centimeter scale (Fig. 4) corroborate the differences between the first 3 layers as well as the correlation between SOM and water, i.e. the higher the content of water, the higher the content of SOM. Layers D1-2 and D2-2, displaying the same characteristics, will be referenced as the WSL (whitish

443 silt loam) layer. Note that this particular WSL layer was not observed in the U1 soil core (Fig.
444 2).

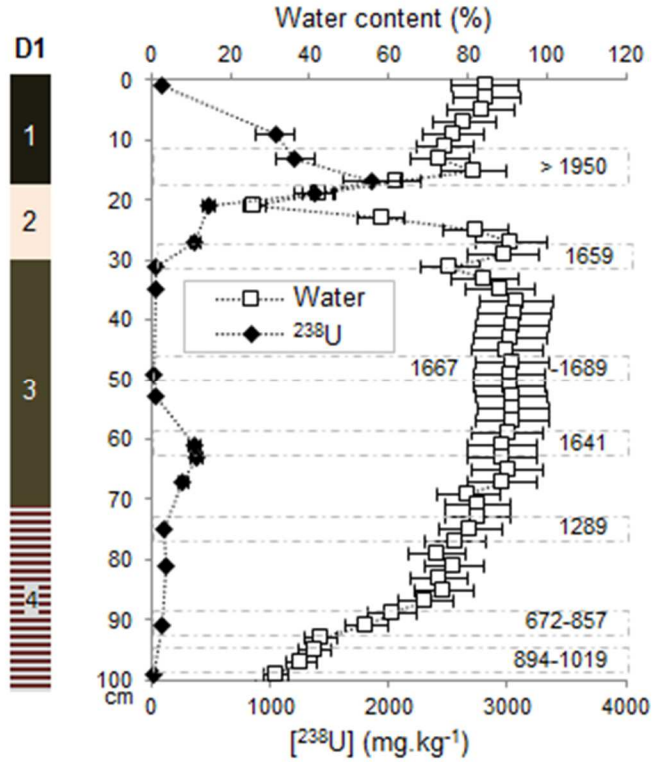

445

446 Fig. 3: Simplified soil profile description of core D1 (100 cm) with water content, ^{238}U concentrations
447 in dry mass and with ^{14}C dating.

448 ***4.3.2. Uranium depth profiles and distribution in the watershed***

449 The U concentrations determined range from 8.9 to 3,560 mg.kg^{-1} in dry mass for cores D1
450 and D2 (Fig. 3 and Fig. 4). An analysis of the U soil profile for the D1 core reveals a U
451 concentration increase between the D1-1 and D1-2 layers (10-20 cm) for the highest
452 concentration (i.e. 1,855 mg.kg^{-1}) and a smaller rise at the end of the D1-3 layer (379 mg.kg^{-}
453 ^{1}). The D1-4 layer exhibits a low U concentration of around 10 mg.kg^{-1}, which is in agreement
454 with the local geological background (11-59 mg.kg^{-1}, from (Salpeteur and Angel, 2010)).
455 Layers D1-3 and D1-4 can thus be considered as the soil reference before the period of
456 mining operations. The higher spatial resolution of core D2 over 30 cm highlights two U

peaks at the interface between D2-1/2, in accordance with D1 results, and in the lower part of D2-2 (not visible on D1 results), with respective intensities of 1,800 mg.kg^{-1} and 3,560 mg.kg^{-1}. By considering the density and water content of each soil layer, the highest mass of U is primarily stored in the WSL layer (D1-2 and D2-2), with a tendency to accumulate locally at the interface with the topsoil layers (D1-1 and D2-1) characterized by a high SOM content.

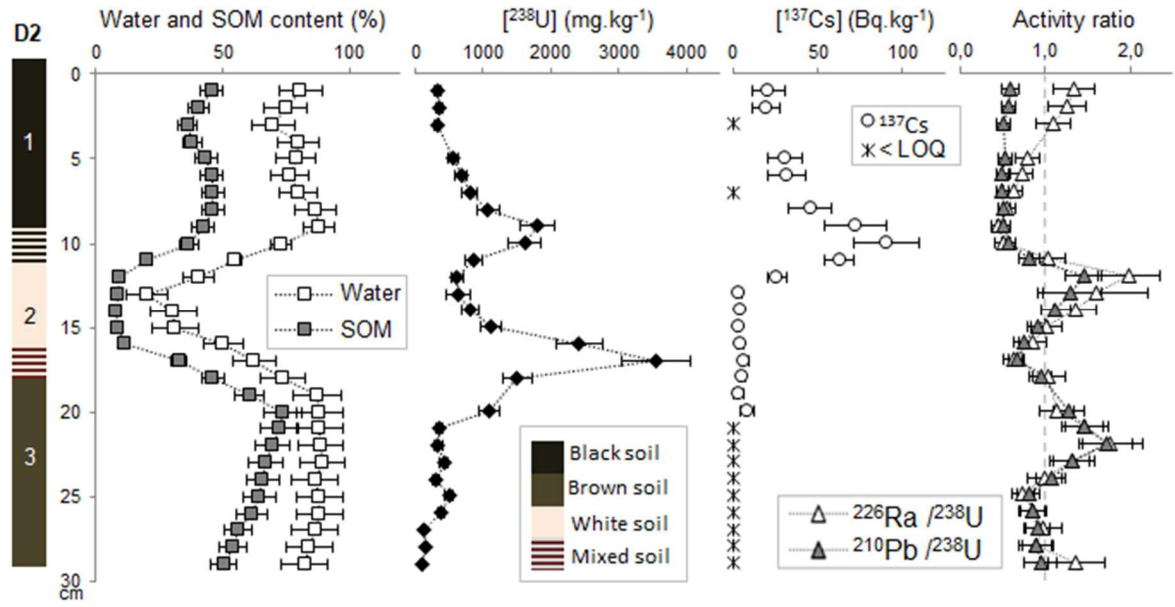

Fig. 4: Simplified soil profile description of core D2 (30 cm) with water and SOM contents, ^{238}U concentrations in dry mass, ^{137}Cs activity in dry mass (LOQ : Limit of Quantification) and activity ratios of ^{226}Ra and ^{210}Pb to ^{238}U.

This correlation between U stock and WSL layer was confirmed by the M-series of 50-cm cores in the area (Fig. S9), which also indicated the presence of the WSL layer, mainly in the center of the watershed downstream of the mine discharge location. Moreover, the U soil profile concentrations of the U1 core (not shown here) reveal a single increase in U concentration, from 51 to 77 mg.kg^{-1}, in the organic topsoil layer (0-7 cm); this result is consistent with the absence of the characteristic WSL layer in the first 30 cm.

The measured (^{226}Ra/^{238}U) and (^{210}Pb/^{238}U) activity ratios range from 0.46 to 2.00 and from 0.50 to 1.73, respectively (Fig. 4). Due to the highly distinct mobility of the “long-life”

radionuclides of the ^{238}U decay chain (^{238}U, ^{226}Ra and ^{210}Pb), an activity ratio close to the secular equilibrium highlights a collective transport of radionuclides mainly in particle form (Zielinski et al., 1986), whereas a deviation stands out for an output (by migration) or input (of various origins) of one radionuclide from the decay chain. The ratio value close to 1 at the end of D2-3 is in line with a natural U geological background in secular equilibrium. If we look closely at the results, the second U peak in the lower part of D2-2 correlates with a ratio close to 1, thus suggesting past transport in particulate form. However, an excess of ^{226}Ra and ^{210}Pb observed in the middle of the WSL layer could suggest a depletion in U. The D2-1 layer with the first U peak shows a continuous deviation from 0.46 at 10 cm to 1.34 at the soil surface for the $^{226}Ra/^{238}U$ ratio, in comparison with the $^{210}Pb/^{238}U$ ratio of around 0.5. This difference in behavior combined with the deviation from a ratio of 1 signifies a rupture in the decay chain between ^{226}Ra and ^{210}Pb and a non-equilibrium with ^{238}U. The $^{226}Ra/^{238}U < 1$, at the end of the D2-1 layer, may highlight the input of ^{238}U into this soil layer by means of a vertical migration from the WSL layer (D2-2).

In addition, SEM has revealed the presence of a large number of U-rich particles with diameters between 1 and 20 µm in the D2-1 and D2-2 layers of the core (Fig. S6). The EDS spectra show the presence of U at contents as high as 50% and an association with other elements (Pb, Fe, Cu. Al, Si and O).

4.3.3. Tracers: ^{14}C, ^{137}Cs and stable lead isotopy

^{14}C dating results on core D1, as detailed in Table S11 and summarized in Fig. 3, show a post-1950 age for the depths 12-14 and 16-18 cm. The sample at depths of 20-22 cm (aliquoted in WSL) could not be dated by the ^{14}C dating technique since it was devoid of carbon. From 30

to 100 cm, older ages of up to 1 millennium are involved. The dating step has been refined over the first 30 cm via ^{137}Cs on core D2 (Fig. 4).

Cesium makes it possible to date sediments by their ^{137}Cs activity caused by nuclear fallout (IAEA, 1998, p.6) combined with their limited mobility properties. The specific ^{137}Cs activity in the D2-1 layer reaches an intermediate value of 31.7 $Bq.kg^{-1}$ at 6 cm, and a maximum of 91 $Bq.kg^{-1}$ was observed right at the D2-1/2 interface (Fig. 4). The values then decrease to roughly 3.4 $Bq.kg^{-1}$ for the lower parts of the D2-2 and D2-3 layers. Below 20 cm, the values were less than the limit of detection. Since the main peak of ^{137}Cs activity in the D2 core is located directly above the WSL layer and only very low values were detected below, it seems safe to assume that this layer was deposited before the peak in nuclear weapons testing at the beginning of the 1960's (IAEA, 1998, p.45). Moreover, this finding is consistent with ^{14}C dating for this layer (post-1950 age).

The benefit of using stable lead isotopes (Fig. 5) is to both highlight the existence of an environmental marker related to the presence of U and discriminate between anthropogenic (uranium stemming from mining and milling activities) and natural input (uranium from the geochemical background). Most stable Pb isotopes are indeed present in the decay chains of naturally occurring radionuclides (^{238}U -> ^{206}Pb, ^{235}U -> ^{207}Pb and ^{232}Th -> ^{208}Pb) and moreover ^{204}Pb is non-radiogenic.

Our data are shown in a three-isotope diagram ($^{207}Pb/^{206}Pb$ vs. $^{204}Pb/^{206}Pb$, Fig. 5a), thus showcasing the mixing processes between various pollution sources. For purposes of comparison, the A64 sample (Loire surface sediment 47°17'17"N - 02°10'54"W (Péron *et al.*, 2016), which is not under the influence of mining discharges) was used as the geochemical background end-member with a $^{207}Pb/^{206}Pb$ ratio (0.859 ± 0.001) close to the Present Day

519 Average Crustal (PDAC) $^{207}Pb/^{206}Pb$ ratio estimated at 0.83 (Cumming and Richards, 1975;
520 Stacey and Kramers, 1975). As observed in Figure 4a, the alignment of the samples (R^2 =
521 0.9999) confirms a binary mixing between the U-ore particles and the geochemical
522 background. This outcome clearly highlights an anthropogenic signature in the recent core
523 layers, in comparison with the PDAC and A64, which are consistent with a post-mining
524 context. In order to calculate the radiogenic Pb contribution in the core samples, a precise
525 determination of the Pb end-members is of great importance. The A64 sample was used for
526 the geochemical background end-member and for the intercept of the linear regression in
527 Figure 4a as the $^{207}Pb/^{206}Pb$ radiogenic end-member. By applying the mixing model and
528 taking the Pb atomic abundances into account, it is possible to correctly calculate the
529 contribution of radiogenic lead (*k*, in %) to the total lead for each sample (Gourgiotis et al.,
530 2020).

531 The 6 soil samples at a depth below 30 cm (D1-3 and D1-4 layers) present similar $^{207}Pb/^{206}Pb$
532 ratio values, ranging from 0.7664 ± 0.0009 to 0.808 ± 0.001, with 1.4 ± 0.07% < *k* < 1.7 ±
533 0.07% corresponding to a slight U enrichment signature. The soil samples at 12-14 cm (D1-1)
534 and 20-22 cm (top of D1-2) display an intermediate value for both ratios and *k* = 3 ± 0.07%
535 and *k* = 2.7 ± 0.08%, respectively. However, the lowest $^{207}Pb/^{206}Pb$ and $^{204}Pb/^{206}Pb$ ratios
536 were found for the 16-18 cm sample with values of respectively 0.6378 ± 0.0005 and
537 0.04007 ± 0.00005. This sample, with *k* = 8.6 ± 0.07%, is located at the interface between the
538 D1-1 and D1-2 layers in the highest contaminated zone of core D1 ($[U]_{soil}$ between 1,210 and
539 1,850 $mg.kg^{-1}$). These results are in agreement with the $^{207}Pb/^{206}Pb$ ratios obtained for U-
540 contaminated soils and isotopic background in (Cuvier et al., 2016), at 0.6578 and 0.8305,
541 respectively.

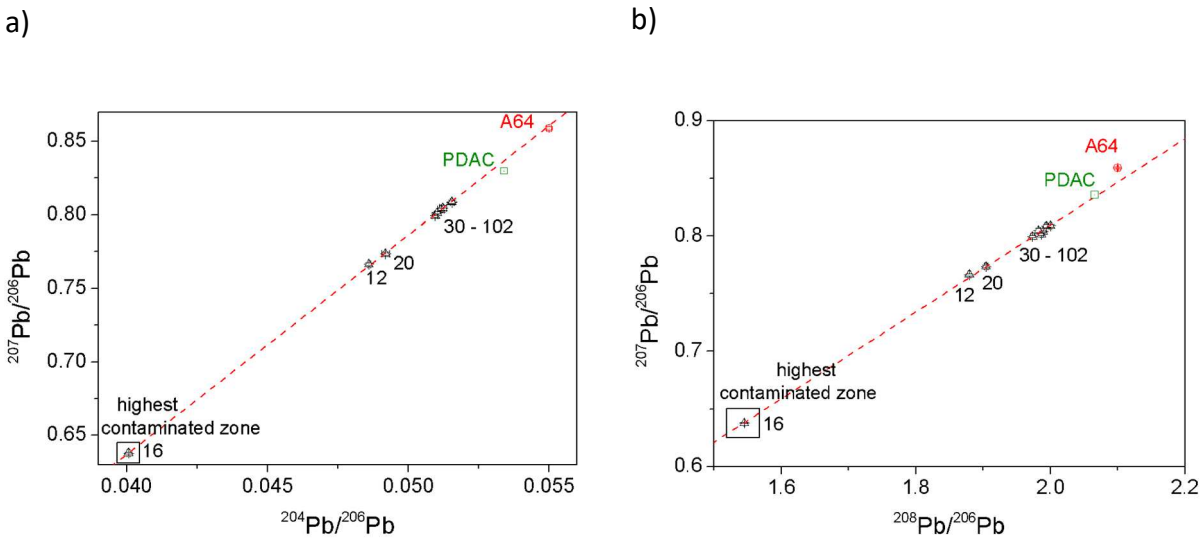

Fig. 5: a) $^{207}Pb/^{206}Pb$ vs. $^{204}Pb/^{206}Pb$ isotope ratios, and b) $^{207}Pb/^{206}Pb$ vs. $^{208}Pb/^{206}Pb$ isotope ratios of core D1. In addition, **A64,** Loire Surface sediment and **PDAC** (Present Day Average Crustal Ratios) (Cumming and Richards, 1975; Stacey and Kramers, 1975) have been plotted. The dashed line represents the linear regression. The uncertainties (2σ) are included in the plot. The values indicated under the points correspond to the depths (in cm). The 30-102 cm range includes 6 sampling depths, namely 30, 48, 60, 74, 90 and 102 cm.

The $^{207}Pb/^{206}Pb$ vs $^{208}Pb/^{206}Pb$ plot (Fig. 5b) confirms the presence of environmental contamination, mainly due to the presence of U-bearing phases from the U mine, which underscores the absence of thorogenic ^{208}Pb in the U-ore. This observation is consistent with the U-ore minerals of Rophin previously described, which are lacking in ^{232}Th. The linear regression (R^2 = 0.9996) indeed indicates binary mixing with no supply of ^{208}Pb in the highest contaminated zone. The highest contaminated zone (16-18 cm sample) has the lowest $^{208}Pb/^{206}Pb$ ratio: 1.5451 ± 0.0009. In a post-U mining context, the results are consistent (^{238}U to ^{206}Pb) with the geochemical background A64 $^{208}Pb/^{206}Pb$ ratio: 2.100 ± 0.001. These results are also in agreement with the isotopic background ($^{208}Pb/^{206}Pb$ = 2.09) and U-contaminated soils ($^{208}Pb/^{206}Pb$ = 1.620) obtained in (Cuvier et al., 2016). The $^{208}Pb/^{206}Pb$ ratio indicates that the enrichment matches with an uranogenic and not thorogenic Pb. The

other depths, which correspond to a slight U enrichment signature, present intermediate $^{208}Pb/^{206}Pb$ ratio values ranging from 1.8795 ± 0.0009 to 2.000 ± 0.001.

4.4. Tree ring analysis

Uranium concentrations measured in the tree rings by HR-ICP-MS are given in Fig. 6; concentrations were detected and quantified in all tree rings analyzed. The distribution patterns of these tree samples reveal different trends.

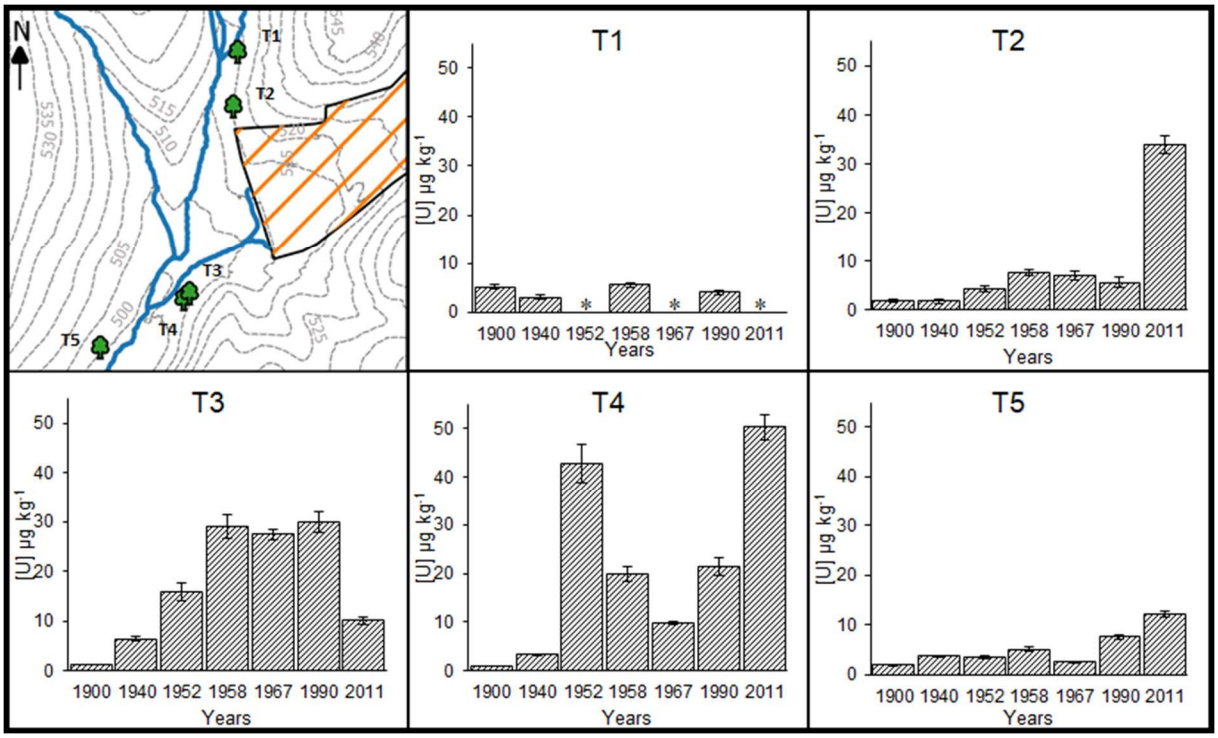

Fig. 6: Locations of the oak trees with contour lines in the Gourgeat watershed (upper left) and uranium concentrations measured in the sampled annual rings

For T5, located far from the former mine without any apparent connection to the watershed due to an elevation difference (Fig. 6), U values ranging from 2 to 12 µg.kg^{-1} were obtained (with low variations over time). For the upstream trees, T1 and T2, U concentrations did not increase over time or only very slightly (except T2 in 2011). The U concentrations found for T1 and T2 during the various years analyzed are of the same order of magnitude, i.e. ranging

575 from 2 to 7 µg.kg^{-1} and up to 34 µg.kg^{-1} for T2 in 2011. The values for trees T3 and T4,
576 located downstream of the storage site, fluctuate strongly over time, from 1 to 50 µg.kg^{-1}
577 with two distinct temporal trends. For T3, the concentration gradually increases until 1990
578 and declines for 2011. For T4, after a maximum concentration measured in 1952, the
579 concentration decreases until 1967 and starts increasing again in 2011.

580 Knowing that the mine was discovered in 1924, the low U concentration values for the year
581 1900 (ranging from 1 to 5 µg.kg^{-1}) are expected to represent the local tree ring background.
582 These backgrounds however are higher than other values given in the literature for oak trees
583 (between 0.3 and 1 µg.kg^{-1}) (Edmands et al., 2001; Monticelli et al., 2009). This finding may
584 be explained by the naturally increasing U levels in the soil (10 mg.kg^{-1}) of areas with granitic
585 bedrock, especially near U deposits.

586 5. Discussion

587 A data integration approach is proposed in this section in order to offer insight into what has
588 actually happened in the Gourgeat watershed. The gamma survey results indicate a
589 contamination in the Gourgeat watershed downstream of the ICPE facility, in contrast with
590 the upstream of the watershed. This finding has been confirmed by the high U
591 concentrations measured in the topsoil (< 30 cm) of cores D1, D2 and the M series. More
592 specifically, the highest U concentrations measured in the soil profiles of cores D1 and D2
593 were localized around the WSL layer (D1-2 and D2-2); this layer with a specific texture, a low
594 water and organic matter content and a high U content was not observed in the U1 core.
595 Such an observation has led to the hypothesis that this contaminated WSL soil layer
596 originated from a natural source or anthropogenic activities located near the current ICPE
597 site. The overlap of gamma survey results with the 1954 aerial photograph (Fig. 2) shows a

partial correlation with a large white surface deposit, visible in the watershed around 200 m downstream of the hydraulic output of the former Rophin settling ponds (deposit not observable in 1946, see Fig. S6). The hypothetical contamination scenario can therefore be refined to a diffuse distribution of natural radionuclides from mine operations transported by water. In other words, the WSL layer could have been deposited in the wetland during a flooding event or else by slow sedimentation as a covering layer of mining materials. This scenario is supported by evidence in the records of: i) ore bodies containing kaolinitic clays (fine particles), ii) malfunction and inadequate maintenance of the settling ponds, and iii) turbid waters with a white coloration in the Gourgeat, Terrasson and Vauziron streams. Moreover, the dating of soil cores D1 and D2 by ^{14}C and ^{137}Cs corroborates the deposit of the WSL post-1950 (for ^{14}C) and before the beginning of the 1960's (for ^{137}Cs), which is in agreement with the timeline (Fig. 1) and the end of mining activities in 1957. In addition, lead isotope ratios indicate that contamination at a depth below 30 cm is slightly influenced by U-mine material (compared to PDCA and A64), while contamination at around 12-22 cm can be distinguished between intermediate and high enrichment signatures with a greater contribution of radiogenic lead to total lead (k = 8.6 ± 0.07%) at 16 cm. Similarly, the enrichment factors, calculated from the mean geochemical background in the D1-3 and D1-4 layers dated prior to 1700 ($[U]_{GB,\ soil}$ = 101 µg.kg^{-1}), range from 3.7 to 35.4 in the WSL layer and from 0.9 to 18.4 in topsoil layers. The WSL layer may thus be used in future studies as a visual tracer during field sampling and as an indicator of a mining activity footprint. Combining this U marking of the wetland with the ^{14}C dating technique, it can be assumed that the wetland is an accumulation area for natural U and its radioactive daughter for up to 1,000 years. This information clearly demonstrates the recent impact of anthropic mining activities not only in the WSL layer but in topsoil layers as well. Following this assessment,

some questions arise, regarding for example the form of transport, and the migration behavior and bioavailability of the radionuclides. The means of transporting radionuclides by turbid waters in the watershed suggests migration in particulate form and most likely as ore particles given the poor efficiency of the ore washing plant process being applied (mainly parsonsite in 1949-1954 and pitchblende in 1955-1957). The measured ratios of the activities of ^{238}U to ^{226}Ra and ^{210}Pb for the U second peak in the lower part of the D2-2 layer (Fig. 4) correlates with a ratio value close to 1, which confirms partial transport as non-altered ore particles. Moreover, SEM (Fig. S8) revealed the existence of U-rich particles in this layer, but the stoichiometry determined by EDS cannot be confirmed with the ore composition of parsonsite or pitchblende. It is therefore assumed that at least a portion of the deposited U mineral particles have dissolved over time. However, disequilibrium in the decay chain for the topsoil layer (D2-1) might suggest an enrichment of U by the migration of U as aqueous species and sorption on SOM. Two hypothesis can be formulated: i) a slow dissolution of U particles contained in the WSL layers over decades, followed by an accumulation in the topsoil layer associated with a seasonal change of water level in the wetland; or ii) a regular inflow over the decades of U dissolved by water from the Gourgeat creek altered by mine water effluent even after ICPE site rehabilitations. Such an accumulation mechanism in the wetland has been detected and similarly described for other sites affected by U mining (Bister et al., 2015; Mangeret et al., 2018). At the same time, the fact that U concentrations quickly decrease below the WSL in cores D1 and D2 suggests that the mobility of the U deposited by diffusion has been rather low under the conditions prevailing during the last 50 years. In conclusion, the wetland, enriched in SOM, acts as a radionuclide trap for natural or anthropogenic U emissions observed at the Rophin site over the decades.

In this study, the dendroanalysis has served to correlate the U emissions from Rophin with the site history using oak tree rings as a suitable bioindicator of changes in bioavailable U concentrations. Considering the local tree ring background observed in 1900, two U concentration variations between 1940 and 2011 can be concluded. First, the maximum U values were observed between 1949 and 1958 for the T3 and T4 trees. This increase in U concentration in tree rings coincides with the period of mining activities (1949-1957) with an extended period of influence for T3. This result confirms the past transport of U into the hydraulic system in a bioavailable form. Moreover, by comparing U concentrations in the tree rings of T5 (no hydraulic influence) and T1 and T2 (located upstream) with the T3 and T4 results (located downstream of the former mine and near the effluent waters) for this same period, it is reasonable to assume that this increase could be attributed to mining operations. Such anthropogenic activities could have generated bioavailable U concentrations, via the documented effluent waters and/or particle deposits (WSL layer), accumulated by the roots of trees growing in the wetland. Let's note that U concentrations in tree rings did not return to the local background level even after mining operations ceased (in 1958). Although an influence on T3 and T4 trees is observed, the concentrations identified are still very low compared to those obtained by Märten et al., (2015) (around 400 $\mu g.kg^{-1}$ for the maximum U concentration). This difference is probably due to both the length of time the site had been in operation (including the processing period) and the quantity of ore extracted. The Rophin site was in fact only operated for 8 years (*vs* 40 years for “Reuster Forst”), including one year of shutdown (in 1951) for economic reasons. This "short" operating period has certainly helped mitigate the impact of these mining activities on plants growing in this region. Second, a large increase in U concentration (more than 20 times the background level) was observed in 2011 for trees T2 and T4. This trend is also slightly visible

669 for the non-influenced T5 tree (6 times). This particular period coincides with the major soil
670 transformations of the Rophin site in 2002 and 2010 (Fig. 1 and Fig. S3), which are visible on
671 the aerial photographs from 1993 to 2015 (Fig. S6). Since the variation was observed on both
672 upstream (T2) and downstream (T4) trees in the vicinity of the ICPE site (and slightly on T5
673 located further away), the hypothesis of an atmospheric contamination during the
674 transformation is indeed possible. The transfer of elements within tree rings is a complex
675 process that depends on a variety of parameters, such as soil pH, soil organic matter,
676 bioavailability, concentrations in the environment, and the uptake capacity of trees (Cutter
677 and Guyette, 1993). Atmospheric contamination during mining is thus one of the pathways
678 of metal transport into trees (Lepp, 1975; Sansone et al., 2001). This determination
679 corresponds mainly to foliar uptake, with subsequent export from the leaf via the phloem,
680 followed by a lateral movement from this tissue into the xylem. However, the relationship
681 between these levels of deposition and the levels in leaves and in other plant parts is
682 presently unknown. On the other hand, this hypothesis is counterbalanced by the T3 tree
683 results, which showed a higher U concentration in 1990 than in 2011.

684 Thanks to our methodology, which employs an integrated approach with a study of records,
685 a gamma survey, and soil and tree ring analyses, it has been possible to trace the
686 contamination history at the Rophin site. Beyond the interest in this methodology, the
687 results of this work will provide the basis for future projects taking place in a ZATU workshop
688 context. Further studies are being planned to better understand the processes taking place
689 in the soil layers in order to derive predictions of the overall dynamics occurring at the site.
690

6. Acknowledgments

The authors are grateful to the ZATU Pilot Workshop within the Hercynian orogeny (ZATU, https://zatu.org/), with the "Nantes-Atlantique Universe Sciences Observatory" (OSUNA, https://osuna.univ-nantes.fr/). The present study has been financially supported by the POLLUSOLS program (OSUNA) and co-financed by the Loire Valley (Pays de la Loire) Regional Council.

Thanks are also extended to Stephan Weiss with the Helmholtz-Zentrum Dresden-Rossendorf, Institute of Resource Ecology, and Guillaume Blain with Subatech for his practical advice concerning the sampling procedure, as well as to Catherine Landesman, Fengqi Xu and Hafid Aglzim with Subatech and Thi-Hong-Hanh Le with the Chemistry Institute of Nice for their valuable assistance during the sampling campaigns.

7. References

Abdelouas, A., 2006. Uranium mill tailings: Geochemistry, mineralogy, and environmental impact. Elements 2, 335–341. https://doi.org/10.2113/gselements.2.6.335

Alessi, D.S., Uster, B., Veeramani, H., Suvorova, E.I., Lezama-Pacheco, J.S., Stubbs, J.E., Bargar, J.R., Bernier-Latmani, R., 2012. Quantitative Separation of Monomeric U(IV) from UO2 in Products of U(VI) Reduction. Environ. Sci. Technol. 46, 6150–6157. https://doi.org/10.1021/es204123z

Ballini, M., Chautard, C., Nos, J., Phrommavanh, V., Beaucaire, C., Besancon, C., Boizard, A., Cathelineau, M., Peiffert, C., Vercouter, T., Vors, E., Descostes, M., 2020. A multi-scalar study of the long-term reactivity of uranium mill tailings from Bellezane site (France). J. Environ. Radioact. 218, 106223. https://doi.org/10.1016/j.jenvrad.2020.106223

Beramendi-Orosco, L.E., Rodriguez-Estrada, M.L., Morton-Bermea, O., Romero, F.M., Gonzalez-Hernandez, G., Hernandez-Alvarez, E., 2013. Correlations between metals in tree-rings of Prosopis julifora as indicators of sources of heavy metal contamination. Appl. Geochemistry 39, 78–84. https://doi.org/10.1016/j.apgeochem.2013.10.003

Bister, S., Birkhan, J., Lüllau, T., Bunka, M., Solle, A., Stieghorst, C., Riebe, B., Michel, R., Walther, C., 2015. Impact of former uranium mining activities on the floodplains of the Mulde River, Saxony, Germany. J. Environ. Radioact. 144, 21–31. https://doi.org/10.1016/J.JENVRAD.2015.02.024

Bollhöfer, A., 2012. Stable lead isotope ratios and metals in freshwater mussels from a uranium mining environment in Australia's wet-dry tropics. Appl. Geochemistry 27,

171–185. https://doi.org/10.1016/J.APGEOCHEM.2011.10.002

Bollhöfer, A., Honeybun, R., Rosman, K., Martin, P., 2006. The lead isotopic composition of dust in the vicinity of a uranium mine in northern Australia and its use for radiation dose assessment. Sci. Total Environ. 366, 579–589. https://doi.org/10.1016/J.SCITOTENV.2005.11.016

Bordelet, G., Beaucaire, C., Phrommavanh, V., Descostes, M., 2018. Chemical reactivity of natural peat towards U and Ra. Chemosphere 202, 651–660. https://doi.org/10.1016/j.chemosphere.2018.03.140

Bretagnolle, V., Benoit, M., Bonnefond, M., Breton, V., Church, J.M., Gaba, S., Gilbert, D., Gillet, F., Glatron, S., Guerbois, C., Lamouroux, N., Lebouvier, M., Mazé, C., Mouchel, J.M., Ouin, A., Pays, O., Piscart, C., Ragueneau, O., Servain, S., Spiegelberger, T., Fritz, H., 2019. Action-orientated research and framework: insights from the French longterm social-ecological research network. Ecol. Soc. 24. https://doi.org/10.5751/ES-10989-240310

Chautard, C., Beaucaire, C., Gerard, M., Roy, R., Savoye, S., Descostes, M., 2020. Geochemical characterization of uranium mill tailings (Bois Noirs Limouzat, France) highlighting the U and 226Ra retention. J. Environ. Radioact. 218. https://doi.org/10.1016/j.jenvrad.2020.106251

Cumberland, S.A., Douglas, G., Grice, K., Moreau, J.W., 2016. Uranium mobility in organic matter-rich sediments: A review of geological and geochemical processes. Earth-Science Rev. 159, 160–185. https://doi.org/10.1016/J.EARSCIREV.2016.05.010

744 Cumming, G.L., Richards, J.R., 1975. Ore lead isotope ratios in a continuously changing earth.
745 Earth Planet. Sci. Lett. 28, 155–171.

746 Cutter, B.E., Guyette, R.P., 1993. Anatomical, Chemical, and Ecological Factors Affecting Tree
747 Species Choice in Dendrochemistry Studies. J. Environ. Qual. 22, 611–619.
748 https://doi.org/10.2134/jeq1993.00472425002200030028x

749 Cuvier, A., Pourcelot, L., Probst, A., Prunier, J., Le Roux, G., 2016. Trace elements and Pb
750 isotopes in soils and sediments impacted by uranium mining. Sci. Total Environ. 566–
751 567, 238–249. https://doi.org/10.1016/J.SCITOTENV.2016.04.213

752 Déjeant, A., Galoisy, L., Roy, R., Calas, G., Boekhout, F., Phrommavanh, V., Descostes, M.,
753 2016. Evolution of uranium distribution and speciation in mill tailings, COMINAK Mine,
754 Niger. Sci. Total Environ. 545–546, 340–352.
755 https://doi.org/10.1016/j.scitotenv.2015.12.027

756 Edmands, J.D., Brabander, D.J., Coleman, D.S., 2001. Uptake and mobility of uranium in black
757 oaks: Implications for biomonitoring depleted uranium-contaminated groundwater.
758 Chemosphere 44, 789–795. https://doi.org/10.1016/S0045-6535(00)00376-3

759 Gourgiotis, A., Mangeret, A., Manhès, G., Blanchart, P., Stetten, L., Morin, G., Le Pape, P.,
760 Lefebvre, P., Le Coz, M., Cazala, C., 2020. New Insights into Pb Isotope Fingerprinting of
761 U-Mine Material Dissemination in the Environment: Pb Isotopes as a Memory
762 Dissemination Tracer. Environ. Sci. Technol. 54, 797–806.
763 https://doi.org/10.1021/acs.est.9b04828

764 Greffoy, J., Sarcia, J.A., 1955. Contribution à l'Etude des Pechblendes Françaises.

765 Guiollard, P.-C., 2002. L'uranium du Morvan et du Forez.

766 Hagemeyer, J., 2000. Chapter 13 Trace metals in tree rings: what do they tell us? Trace Met.
767 Environ. 4, 375–385. https://doi.org/10.1016/S0927-5215(00)80016-8

768 Hassan Loni, Y., David, K., Larrue, S., Grambow, B., Corona, C., Ribet, S., Chardon, P.,
769 Montavon, G., 2019. Uranium quantification of oak tree rings (Quercus petraea) from a
770 former uranium mining site by High Resolution Inductively Coupled Plasma Mass
771 spectrometry in Laser Ablation and Solution modes. Spectrochim. Acta - Part B At.
772 Spectrosc. 161, 105709. https://doi.org/10.1016/j.sab.2019.105709

773 Heiri, O., Lotter, A.F., Lemcke, G., 2001. Loss on ignition as a method for estimating organic
774 and carbonate content in sediments: reproducibility and comparability of results. J.
775 Paleolimnol. 25, 101–110. https://doi.org/10.1023/A:1008119611481

776 Himeur, N., 2010. Bilan environnemental sites miniers de du Puy-de-Dôme.

777 Himeur, N., Andres, C., 2012. Suivi environnemental du site de Rophin - communes de
778 Lachaux et Ris.

779 IAEA, 1998. 137Cs use in estimating soil erosion: 30 years of research. IAEA TECDOC-1028.
780 Int. At. Energy Agency 13–16.

781 IRSN, 2018. IRSN MIMAUSA database, Memory and Impact of uranium mines: synthesis and
782 records [WWW Document]. URL https://mimausabdd.irsn.fr/

783 IRSN, 2014. Report on the Radiological State of the Environment in France in 2010-2011.

784 Jonsson, A., Eklund, M., Håkansson, K., 1997. Heavy Metals of the 20th Century Recorded in

785 Oak Tree Rings. J. Environ. Qual. 26, 1638.
786 https://doi.org/10.2134/jeq1997.00472425002600060025x

787 Larsson, 2016. CDendro & CooRecorder Program Package for Tree Ring Measurements and
788 Crossdating of the Data [WWW Document]. URL http://www.cybis.se/forfun/dendro/

789 Le Berre, S., Bretesché, S., 2019. Having a high-risk job: Uranium miners' perception of
790 occupational risk in France. Extr. Ind. Soc. https://doi.org/10.1016/J.EXIS.2019.11.011

791 Lepp, N.W., 1975. The potential of tree-ring analysis for monitoring heavy metal pollution
792 patterns. Environ. Pollut. 9, 49–61. https://doi.org/10.1016/0013-9327(75)90055-5

793 Li, D., Seaman, J.C., Chang, H.-S., Jaffe, P.R., Koster van Groos, P., Jiang, D.-T., Chen, N., Lin, J.,
794 Arthur, Z., Pan, Y., Scheckel, K.G., Newville, M., Lanzirotti, A., Kaplan, D.I., 2014.
795 Retention and chemical speciation of uranium in an oxidized wetland sediment from
796 the Savannah River Site. J. Environ. Radioact. 131, 40–46.
797 https://doi.org/10.1016/J.JENVRAD.2013.10.017

798 Ljungberg, J., Öhlander, B., 2001. The geochemical dynamics of oxidising mine tailings at
799 Laver, northern Sweden. J. Geochemical Explor. 74, 57–72.
800 https://doi.org/https://doi.org/10.1016/S0375-6742(01)00175-3

801 Lottermoser, B.G., Ashley, P.M., 2005. Tailings dam seepage at the rehabilitated Mary
802 Kathleen uranium mine, Australia. J. Geochemical Explor. 85, 119–137.
803 https://doi.org/10.1016/j.gexplo.2005.01.001

804 Lovley, D.R., Phillips, E.J.P., Gorby, Y.A., Landa, E.R., 1991. Microbial reduction of uranium.
805 Nature 350, 413–416. https://doi.org/10.1038/350413a0

Mangeret, A., Blanchart, P., Alcalde, G., Amet, X., Cazala, C., Gallerand, M.-O., 2018. An evidence of chemically and physically mediated migration of 238U and its daughter isotopes in the vicinity of a former uranium mine. J. Environ. Radioact. 195, 67–71. https://doi.org/10.1016/J.JENVRAD.2018.08.018

Märten, A., Berger, D., Köhler, M., Merten, D., 2015. The dendroanalysis of oak trees as a method of biomonitoring past and recent contamination in an area influenced by uranium mining. Environ. Sci. Pollut. Res. 22, 19417–19425. https://doi.org/10.1007/s11356-015-4902-z

Mikutta, C., Langner, P., Bargar, J.R., Kretzschmar, R., 2016. Tetra- and Hexavalent Uranium Forms Bidentate-Mononuclear Complexes with Particulate Organic Matter in a Naturally Uranium-Enriched Peatland. Environ. Sci. Technol. 50, 10465–10475. https://doi.org/10.1021/acs.est.6b03688

Monticelli, D., Di Iorio, A., Ciceri, E., Castelletti, A., Dossi, C., 2009. Tree ring microanalysis by LA-ICP-MS for environmental monitoring: Validation or refutation? Two case histories. Microchim. Acta 164, 139–148. https://doi.org/10.1007/s00604-008-0049-7

Nabaisa, C., Freitasa, H., Hagemeyerb, J., 1999. Dendroanalysis: A tool for biomonitoring environmental pollution? Sci. Total Environ. 232, 33–37. https://doi.org/10.1016/S0048-9697(99)00107-2

Nakashima, S., Disnar, J.R., Perruchot, A., Trichet, J., 1984. Experimental study of mechanisms of fixation and reduction of uranium by sedimentary organic matter under diagenetic or hydrothermal conditions. Geochim. Cosmochim. Acta 48, 2321–2329. https://doi.org/10.1016/0016-7037(84)90228-X

828 Newsome, L., Morris, K., Shaw, S., Trivedi, D., Lloyd, J.R., 2015. The stability of microbially
829 reduced U(IV); impact of residual electron donor and sediment ageing. Chem. Geol.
830 409, 125–135. https://doi.org/10.1016/J.CHEMGEO.2015.05.016

831 Owen, D.E., Otton, J.K., 1995. Mountain wetlands: Efficient uranium filters — potential
832 impacts. Ecol. Eng. 5, 77–93. https://doi.org/10.1016/0925-8574(95)00013-9

833 Pearson, C., Manning, S.W., Coleman, M., Jarvis, K., 2005. Can tree-ring chemistry reveal
834 absolute dates for past volcanic eruptions? J. Archaeol. Sci. 32, 1265–1274.
835 https://doi.org/10.1016/J.JAS.2005.03.007

836 Péron, O., Gégout, C., Reeves, B., Rousseau, G., Montavon, G., Landesman, C., 2016.
837 Anthropogenic tritium in the Loire River estuary, France. J. Sea Res. 118, 69–76.
838 https://doi.org/10.1016/j.seares.2016.04.003

839 Perone, A., Cocozza, C., Cherubini, P., Bachmann, O., Guillong, M., Lasserre, B., Marchetti,
840 M., Tognetti, R., 2018. Oak tree-rings record spatial-temporal pollution trends from
841 different sources in Terni (Central Italy). Environ. Pollut. 233, 278–289.
842 https://doi.org/10.1016/J.ENVPOL.2017.10.062

843 Ramsey, C.B., 2017. Methods for Summarizing Radiocarbon Datasets. Radiocarbon 59, 1809–
844 1833. https://doi.org/10.1017/RDC.2017.108

845 Regenspurg, S., Margot-Roquier, C., Harfouche, M., Froidevaux, P., Steinmann, P., Junier, P.,
846 Bernier-Latmani, R., 2010. Speciation of naturally-accumulated uranium in an organic-
847 rich soil of an alpine region (Switzerland). Geochim. Cosmochim. Acta 74, 2082–2098.
848 https://doi.org/10.1016/J.GCA.2010.01.007

Reimer, P.J., Bard, E., Bayliss, A., Beck, J.W., Blackwell, P.G., Ramsey, C.B., Buck, C.E., Cheng, H., Edwards, R.L., Friedrich, M., Grootes, P.M., Guilderson, T.P., Haflidason, H., Hajdas, I., Hatté, C., Heaton, T.J., Hoffmann, D.L., Hogg, A.G., Hughen, K.A., Kaiser, K.F., Kromer, B., Manning, S.W., Niu, M., Reimer, R.W., Richards, D.A., Scott, E.M., Southon, J.R., Staff, R.A., Turney, C.S.M., van der Plicht, J., 2013. IntCal13 and Marine13 Radiocarbon Age Calibration Curves 0–50,000 Years cal BP. Radiocarbon 55, 1869–1887. https://doi.org/DOI: 10.2458/azu_js_rc.55.16947

Reyss, J.L., Mangeret, A., Courbet, C., Bassot, S., Alcalde, G., Thouvenot, A., Guillevic, J., 2016. Estimation of sedimentation rates based on the excess of radium 228 in granitic reservoir sediments. J. Environ. Radioact. 162–163, 8–13. https://doi.org/10.1016/j.jenvrad.2016.04.032

Salpeteur, I., Angel, J.-M., 2010. Geochemical baseline data for trace elements in surface water and active sediment from French rivers collected by the FOREGS Geochemical Atlas of Europe (I). Environnement, Risques & Santé 9, 121–135. https://doi.org/10.1684/ers.2010.0332

Sansone, U., Roberto Danesi, P., Barbizzi, S., Belli, M., Campbell, M., Gaudino, S., Jia, G., Ocone, R., Pati, A., Rosamilia, S., Stellato, L., 2001. Radioecological survey at selected sites hit by depleted uranium ammunitions during the 1999 Kosovo conflict. Sci. Total Environ. 281, 23–35. https://doi.org/10.1016/S0048-9697(01)01034-8

Schöner, A., Noubactep, C., Sauter, M., 2009. Geochemistry of natural wetlands in former uranium milling sites (eastern Germany) and implications for uranium retention. Geochemistry 69, 91–107. https://doi.org/10.1016/J.CHEMER.2007.12.003

871 Stacey, J.S., Kramers, J.D., 1975. Approximation of terrestrial lead isotope evolution by a
872 two-stage model. Earth Planet. Sci. Lett. 26, 207–221. https://doi.org/10.1016/0012-
873 821X(75)90088-6

874 Tedjani, A., Mavon, C., Belafrites, A., Degrelle, D., Boumala, D., Rius, D., Groetz, J.-E., 2016.
875 Well GeHP detector calibration for environmental measurements using reference
876 materials. Nucl. Instruments Methods Phys. Res. Sect. A Accel. Spectrometers, Detect.
877 Assoc. Equip. 838, 12–17. https://doi.org/10.1016/J.NIMA.2016.09.022

878 Wang, Y., Bagnoud, A., Suvorova, E., McGivney, E., Chesaux, L., Phrommavanh, V., Descostes,
879 M., Bernier-Latmani, R., 2014. Geochemical Control on Uranium(IV) Mobility in a
880 Mining-Impacted Wetland. Environ. Sci. Technol. 48, 10062–10070.
881 https://doi.org/10.1021/es501556d

882 Watmough, S.A., Hutchinson, T.C., 1996. Analysis of tree rings using inductively coupled
883 plasma mass spectrometry to record fluctuations in a metal pollution episode. Environ.
884 Pollut. 93, 93–102. https://doi.org/10.1016/0269-7491(95)00107-7

885 Zielinski, R.A., Bush, C.A., Rosholt, J.N., 1986. Uranium series disequilibrium in a young
886 surficial uranium deposit, northeastern Washington, U.S.A. Appl. Geochemistry 1, 503–
887 511. https://doi.org/10.1016/0883-2927(86)90055-7

888